

Evolution of surface damage of thin film composite (TFC) reverse osmosis (RO) membranes under controlled hygro-mechanical conditions

Abedalkader Alkhouzaam, Fatima Ghassan Alabtah, Marwan Khraisheh

Item type

Journal Contribution

Terms of use

This work is licensed under a [CC BY 4.0](#) license

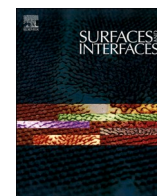
This version is available at

https://manara.qnl.qa/articles/journal_contribution/Evolution_of_surface_damage_of_thin_film_composite_TFC_reverse_osmosis_mechanical_conditions/23092247/2

Access the item on Manara for more information about usage details and recommended citation.

Posted on Manara – Qatar Research Repository on

2023-07-01



Evolution of surface damage of thin film composite (TFC) reverse osmosis (RO) membranes under controlled hygro-mechanical conditions

Abedalkader Alkhouzaam, Fatima Ghassan Alabtah, Marwan Khraisheh *

Mechanical Engineering Program, Texas A&M University at Qatar, Qatar

ARTICLE INFO

Keywords:

Thin-film composite (TFC) membranes
Mechanical integrity
TFC stability
Surface characterization
Interrupted mechanical testing

ABSTRACT

Limited attention has been given to understanding how failure to the selective layer of reverse osmosis (RO) membranes develops and accumulates during operation; and to integrating this response into membrane fabrication. While the integrity of the selective layer is crucial for the separation process, available studies are limited to simple loading conditions and use failure of the entire membrane at rupture to represent its mechanical integrity. This work aims to investigate the evolution of surface damage to the selective layer under controlled interrupted mechanical tests under dry and wet conditions. AFM, SEM, and contact angle are used to characterize the selective layer integrity. Wet membranes exhibited lower strain at rupture (10.3%) than that of dry membranes (12.3%). However, interrupted tests revealed that the failure of the selective layer occurred at much lower strains than the rupture strain. Stretching and thinning in the TFC layer were observed at strain limits as low as 5%, which developed into localized deformation and cracks at higher strain limits (i.e., 8%). These findings can explain why membranes fail to perform before rupture occurs. By understanding how the selective layer's surface damage evolves during operation, membrane fabrication can be improved to enhance membrane performance and durability.

1. Introduction

Scarcity and global demand of freshwater have made the accessibility to clean and safe water resources one of the major global grand challenges now and in the future. As the water management strategies of various countries continue to evolve, desalination is becoming an integral part of their efforts [1]. Non-conventional water sources like seawater and brackish water are now considered vital for low-cost production of freshwater [2]. In the effort toward a sustainable recovery of freshwater from saline water, membrane-based technologies have gained the interest and acceptance of the scientific community worldwide owing to their distinct features over the conventional desalination technologies [3]. Membranes can be easily fabricated, processed, and tailored to suit the desired application, making them a flourishing research area in academia. On the other hand, their antifouling properties, chemical and mechanical stabilities need further enhancements to maintain membrane performance under harsh conditions and for long operational periods [4]. Huge efforts are being made to develop high antifouling membranes with high chemical stability [5,6]. In contrast, less efforts are focused on their mechanical stability and behavior under

harsh and complex conditions.

Among the various membrane types and configurations, thin-film composite (TFC) membranes have proven their high efficiency in nanofiltration (NF), reverse osmosis (RO), forward osmosis (FO), and pressure retarded osmosis (PRO) [7,8]. TFC membranes are generally fabricated via the interfacial polymerization (IP) reaction of two monomers to form a thin-film selective layer. TFC membranes consist of three layers: a reinforcing nonwoven backing (e.g., polyester) to provide a mechanical support for high-pressure processes, a porous layer like polysulfone (PSF) that acts as a platform for the IP reaction, and a thin polyamide (PA) layer that controls the separation (Fig. 1) [9,10]. Although TFC membranes possess high separation efficiency, they are susceptible to deform in pressure-driven processes due to different compressional, bending, and elongational stresses [11]. Although these membranes are reinforced by a non-woven backing layer, the thin selective layer (i.e., TFC) and the porous substrate layer may deform when subjected to high hydraulic pressure for long operational periods leading to a partial or complete membrane failure. Moreover, TFC membranes are usually subjected to varying and harsh conditions during normal operations, physical and chemical cleaning, vibrations, and high cross-flow velocities [12]. The high crossflow velocity, i.e., the linear velocity

* Corresponding author.

E-mail address: marwan.khraisheh@qatar.tamu.edu (M. Khraisheh).

<https://doi.org/10.1016/j.surfin.2023.102911>

Received 17 January 2023; Received in revised form 16 April 2023; Accepted 26 April 2023

Available online 6 May 2023

2468-0230/© 2023 The Authors. Published by Elsevier B.V. This is an open access article under the CC BY license (<http://creativecommons.org/licenses/by/4.0/>).

Nomenclature

TFC	thin-film composite	PVDF	polyvinylidene difluoride
UF	ultrafiltration	IP	interfacial polymerization
NF	nanofiltration	NIPS	non-solvent induced phase separation (phase inversion)
RO	reverse osmosis	PA	polyamide
FO	forward osmosis	PET	polyethylene terephthalate
PRO	pressure retarded osmosis	PEI	polyetherimide
CA	contact angle (°)	PAI	polyamide-imide
SEM	scanning electron microscope	PE	polyethylene
AFM	atomic force microscopy	PDA	polydopamine
PES	polyethersulfone	DPE	polydopamine-modified polyethylene
PSF	polysulfone	TA	tannic acid
PVA	polyvinyl alcohol	APTES	3-aminopropyltriethoxysilane
PAN	polyacrylonitrile	SPSF	sulfonated polysulfone
PS	polyester	TPE	TA-APTES-coated PE substrate
		PDMA	pendant drop mechanical analysis

of the tangential flow, along with the high operational pressures may significantly influence the integrity of the TFC layer that controls the separation. The stability and mechanical integrity of the TFC layer depends on various factors including the materials selection (monomers and fillers) during fabrication, the adhesion properties with the middle layer (the porous substrate), properties of the middle layer (porosity, thickness, compactibility, pore size and structure), and the nonwoven backing [13,14].

Efforts in investigating and optimizing the mechanical stability and integrity of TFC membranes are rather limited. Indeed, due to the complex loads and stresses applied accompanied with the sensitivity of the TFC layer, TFC membranes tend to undergo severe deformations. Some studies in the literature explored new ways of enhancing or investigating the mechanical strength of TFC membranes. These studies usually report the mechanical strength in terms of the tensile strength, elongation, and Young's modulus at complete membrane rupture including the supporting layers (i.e., the nonwoven backing and the middle layers) [11,15,16]. Therefore, many studies have proposed new materials and techniques to enhance the support layer strength aiming to fabricate a mechanically stable membrane. However, enhancing the mechanical strength of the supporting layers doesn't necessarily enhance the TFC layer stability and integrity. For example, some studies proposed the deposition of TFC layer on a polyethylene (PE) substrates that have less thickness and higher mechanical strength compared to conventional supports [17]. PE-based substrates could achieve three times higher tensile strength and elongation at break compared to conventional substrates like polysulfone (PSF) and polyethersulfone

(PES) [18]. Tian et al. [13] fabricated TFC-FO membranes on a double-layer support consisting of electrospun Polyethylene terephthalate-polyvinyl alcohol (PET-PVA) composite and a Polyvinylidene fluoride (PVDF) layer synthesized by the phase inversion method. The authors reported that the mechanical strength represented by the tensile stress at break increases when increasing the polymer concentration owing to the denser structure of substrate. Li et al. [19] fabricated TFC membranes on polyethylenimine (PEI) substrates with different PEI concentrations to evaluate and optimize the mechanical stability for PRO process. The Young's modulus at break was used to evaluate the overall mechanical strength of the prepared membranes, and the deformation of the TFC layer was evaluated by PRO cyclic experiments. It has been found that the specific salt flux increases dramatically when operated at high pressures (>17 bars) though no obvious change or deformation was observed on the membrane. The increase in salt permeation through the TFC layer suggests a deformation in the TFC layer even before a complete membrane rupture. Other examples of different TFC membranes with different configurations and support layers, and the tests applied to study their mechanical stability are listed in Table 1.

As clearly seen from Table 1, some of these membranes exhibit high strain, which is dominated by the support layers, while no clear investigations on the TFC integrity have been reported by these studies. Efforts in investigating the mechanical strength of the PA layer is much less and was investigated by few studies using the pendant drop mechanical analysis (PDMA). The PDMA technique was first proposed by Greenberg et al. [26], which allows to estimate the mechanical strength

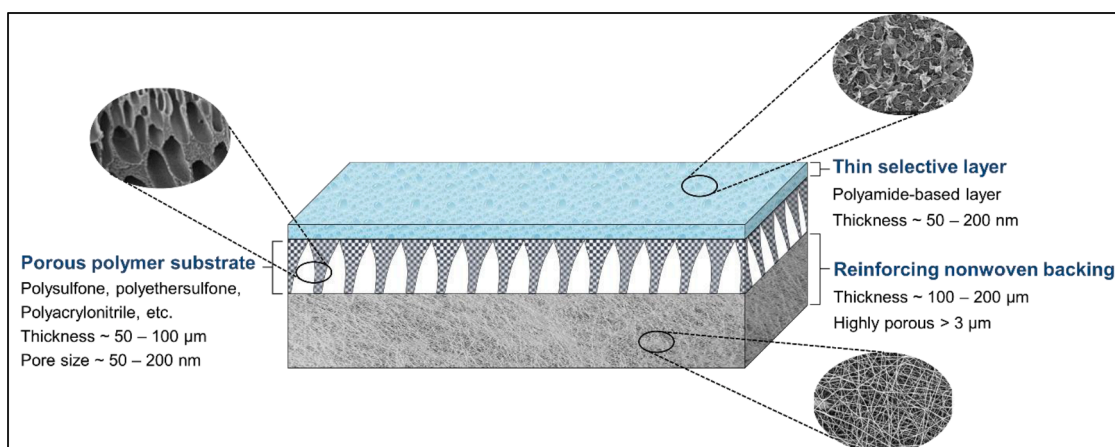


Fig. 1. Illustration showing the common structure of the TFC membranes.

Table 1

The reported TFC membranes in the literature, supporting layers, and the mechanical tests used.

TFC Membrane	TFC Supporting layers	Mechanical test	strain at break (%)	Ref.
ZnO-TiO ₂ /PA/PSF ^a	Porous PSF substrate fabricated by NIPS approach.	Young's modulus, tensile strength, and strain at break	44*	[1]
PA/PAI/PS	Porous PAI layer fabricated by NIPS approach with reinforcing nonwoven PS fabric.	Young's modulus, tensile strength, and strain at break. Effect of compaction (in dead-end filtration cell) on membrane thickness.	6.1 ± 0.4	[11]
PA/PVDF/PET-PVA	Porous (PVDF) layer fabricated by NIPS approach on a composite nanofibrous layer (PET-PVA) fabricated by electrospinning.	Young's modulus and tensile strength at break	–	[13]
PA/PAN/PS	Porous PAN substrate fabricated by NIPS approach with reinforcing nonwoven PS fabric.	Young's modulus, Tensile strength, and strain at break	14 ± 3.7	[15]
PA/TPE	Porous PE substrate coated by the co-deposition of TA and APTES.	Young's modulus, Tensile strength, and strain at break	53 ± 5	[17]
PA/PE	Porous PE substrate	Young's modulus, tensile strength, and strain at break	50 ± 4	[18]
PA/PEI/m-SiO ₂	Porous substrate (PEI/m-SiO ₂) fabricated by NIPS approach.	Tensile strength at break	–	[20]
PA/PET	Nanofibrous substrate (PET) fabricated by electrospinning.	Tensile strength and strain at break	135*	[21]
PA/DPE	PDA-coated PE substrate.	Young's modulus, tensile strength, and strain at break	74 ± 3	[22]
PA/PSF/PET	Porous PSF substrate fabricated by NIPS approach with reinforcing woven PET fabric.	Young's modulus, tensile strength, and strain at break	39 ± 7	[23]
PA/PSF-SPSF/PET	Porous PSF-SPSF substrate fabricated by NIPS approach with reinforcing nonwoven PET fabric.	Young's modulus and tensile strength at break	–	[24]
PA/PEI	Porous PEI substrate fabricated by NIPS approach.	Young's modulus at break and cyclic PRO experiments at varying pressures.	–	[19]
PA/PVDF-SiO ₂	Composite nanofibrous substrate (PVDF-SiO ₂) fabricated by electrospinning.	Young's modulus, tensile strength, and strain at break	375*	[25]

^a The PA layer was coated with ZnO-TiO₂ nanocomposite layer.

* Strain% was estimated from the stress-strain curve.

of a PA layer formed on a drop surface by injecting more liquid into the drop until it deforms. The mechanical properties of the formed PA layer can be then estimated by the drop size and the internal pressure increase. Using the PDMA technique, Roh et al. [27] found that the rupture strength of the PA layer is highly affected by the monomer concentrations used during the IP reaction conditions. Wang et al. [28] investigated the effect of polyisobutylene (PIB) embedding into the PA composite on its mechanical strength using the PDMA method. Different from Greenberg et al. and Roh et al. studies, the PA layer was not formed

onto a liquid drop, but was stripped by dissolving the support PSF substrate using *n,n*-dimethylformamide (DMF) solvent. The PDMA approach provided useful insights onto the relationship between the PA forming conditions and its mechanical response. However, the major limitation of this method is the difficulty of PA formation on the surface of a liquid drop or the PA stripping using organic solvents. Another concern develops here is the possibility of PA deformation during the PA isolation and transferring to the PDMA apparatus. Moreover, the mechanical integrity of the PA layer is influenced by the adhesion properties with the PSF substrate [13,14]. Therefore, analyzing the PA integrity with the entire composite can provide a more comprehensive understanding of its mechanical behavior under operational loads.

TFC membranes can be reinforced by woven [23] or nonwoven fabrics [11,15,24]. In fact, woven and nonwoven backings limit the membrane elongation and exhibit high tensile strength providing higher stability to the other layers. However, they are still stretchable to strain levels at which the TFC and middle layers may deform. The response of the TFC layer to the mechanical load differs from one membrane to another, even if they share the same backing and support layers. This has been demonstrated by Idarraga-Mora et al. [29] where two commercial TFC membranes (SEAMAXX and SW30-XLE) with different properties have been studied. The authors found that the mechanical behavior at fracture was similar for both membranes. However, the effect of the applied strain on their performance was totally different. SEMAXX membranes exhibited up to 50% increase in water and salt permeance after tensile testing. The increase in permeance was attributed to stretching and thinning of the TFC layer and to the possible increase in middle-layer porosity due to the stretching. The increase in salt permeation could be also attributed to damages and cracks in the TFC layer that is highly fragile and may deform at mechanical loads much lower than the loads needed for a complete rupture [30,31]. In contrast, SW30-XLE was less susceptible to deformation providing more stable performance after applying similar mechanical load. These findings suggest that the stability of TFC layers varies from a membrane to another depending on the materials, compositions, and conditions used during the fabrication [13]. Hence, the overall membrane performance may decline even when subjected to stresses lower than its rupture stress, and thus the complete rupture stresses being usually reported does not represent the actual mechanical stability and integrity of a TFC membrane. The high integrity of the TFC layer is necessary to ensure stable performance and less or no damages under external mechanical stresses. Thus, it is necessary to find ways of evaluating the selective layer integrity and stability under mechanical stresses rather than evaluating the overall membrane mechanical strength.

In a recent study [32], we found that the TFC-PA layer exhibits damages and deformations at dynamic stress levels much lower than the static stresses needed for a complete membrane rupture. Moreover, it was established that fatigue deformation is less uniform and is distinguished by the emergence of localized areas with severe deformation. This information suggests that the mechanical integrity of the PA layer at low stress levels should be taken into account when evaluating the mechanical properties of a membrane. The aim of this work is to investigate the evolution of surface characteristics of the TFC layer and assess its integrity at strain levels below the strain-rupture level using controlled interrupted uniaxial tensile testing. The work adds to the relatively small number of literatures that address the mechanical behavior of TFC membranes and PA layer integrity. The mechanical testing of the membrane samples was performed under dry and wet conditions. The evolution and integrity of TFC layer were evaluated using water contact angle, Scanning Electron Microscopy (SEM), and Atomic Force Microscopy (AFM). This study shed new light on the PA layer integrity and its surface characteristics evolve under different conditions and low mechanical stresses. It also gives insights on finding new ways and protocols for mechanical testing of TFC membranes allowing for more accurate predictions of their service life and the development of novel materials and designs to improve their surface

integrity.

2. Experimental methods

2.1. Materials

A commercial RO membrane for brackish water desalination (BW30-LE, FilmTec™) purchased from DuPont, US was used as a model TFC-RO membrane for the conducted analysis. The membrane was tested as received without any chemical modifications. Table 2 lists the manufacturer's specifications and operational limits of the purchased membrane.

2.2. Pre-test samples preparation methods

In accordance with ASTM D638–14, the tensile test specimen was sized to the dimensions shown in Fig. 2(c). The samples were cut using a coherent METABEAM 400 laser cutting system at an 845 mm/s cutting speed and 100 W of power. The membrane samples were then cautiously rinsed and soaked in deionized water (DIW) to remove any preservatives or potential contaminants. The samples were then maintained drying overnight in a clean environment at room temperature to prevent any accidental scratches or contamination. For samples tested in dry conditions, samples were tested directly after overnight drying without further wetting. Two immersion intervals have been used for samples tested under wet conditions: 5 min and overnight immersion, which resulted in 6% and 33% water uptake, respectively. The sample water uptake% was estimated using the gravimetric method [33,34]. In brief, membrane samples were cut into $3 \times 3 \text{ cm}^2$ pieces, washed thoroughly with DIW and dried overnight at room temperature. The dry sample weight was then recorded (W_{dry}). The samples were then immersed in DIW for a specific time (5 min and 24 h) at room temperature. The samples were removed and carefully wiped with a tissue paper to remove excess water on the surface and the wet sample weight was recorded (W_{wet}). The water uptake% was then estimated and averaged from 3 different samples according to Eq. (1):

$$\text{Water uptake (\%)} = \frac{W_{wet} - W_{dry}}{W_{dry}} \times 100\% \quad (\text{Eq. 1})$$

2.3. Tensile samples testing

The tensile testing in this work was carried out using a ZwickRoell customized uniaxial testing apparatus with an environmental chamber. This apparatus is intended to test thin-film materials. The electromechanical actuators can move 200 mm at a maximum speed of 10 mm/s. Along with a 2 kN load cell intended for monitoring static and dynamic tensile and compression forces, each actuator also comes with an on-sided closing screw grip with a 300 N maximum force rating. One uEye camera and an $f = 75 \text{ mm}$ objective lens are positioned at the top with the laserXtens/videotens compact system. An adjustable LED incident light is attached to illuminate the specimen. In this investigation, the system's videoXtens mode was used to evaluate the movement of two marks (targets) on the specimen under dry and wet conditions. The measurement of force conforms with ISO 7500–1 and ASTM E4. Uniaxial tensile studies have been carried out under dry and wet

conditions (room temperature- $22 \pm 1^\circ \text{C}$) up to failure in order to examine the stress-strain behavior of the commercial TFC-RO membranes under various testing settings (Fig. 2(a and b)). The wet testing was conducted using a plexiglass conditioning vessel with a thermoregulation bath. Then interrupted tensile testing for each condition was conducted up to three defined strain limits to determine the effect of loading on surface characteristics evolution as illustrated in Fig. 2(d).

2.4. Characterization

Various analytical techniques have been used to characterize the surface morphology of the unloaded and loaded membranes. All membranes, including the unloaded sample (BW), were cautiously rinsed with DIW and kept drying overnight at room temperature in a clean place prior to characterization. Contact angle analysis was conducted with Goniometer 250-U1 (Ramehart instrument Co.) to evaluate the surface hydrophilicity and uniformity of the stressed and pre-stressed membranes. The analysis was performed at ten different locations at the area between the grips as illustrated in Fig. 3. The Atomic Force Microscopy (AFM) was conducted with Bruker Dimension Icon AFM to evaluate the surface roughness and uniformity of the tested samples. AFM measurements were performed using 512 profile scans over a $5 \times 5 \mu\text{m}^2$ scanned area. The analysis was carried out using the peak force quantitative nanomechanical mapping (QNM) using RTESPA-150–30 probe with a tip radius of 30 nm, length of 125 μm and width of 35 μm . The scanned AFM images were processed in the same way with a first-order flattening. The roughness parameters including the average roughness (R_a), root mean square roughness (RMS or R_q) and the difference in surface area (SAD) were then calculated according to ISO 4288. The effect of mechanical stress on the TFC morphology was assessed by the Scanning Electron Microscopy (SEM). Prior to the SEM analysis, the samples were rinsed with DIW and then dried at room temperature overnight in sterile place to avoid surface contamination or accidental damages. The samples were then coated with a 10 nm platinum layer using the Leica sputter coater (EM ACE600) to enhance the surface conductivity. The SEM images were then obtained at different magnifications via the Apreo-S Thermo Fisher Scientific using an in-lens backscatter detector (T1). The SEM and AFM measurements were performed on the middle area of the narrow region as it is the most affected area of the sample as evidenced by the ruptured samples at which the rupture occurs at the center. Hence, AFM and SEM, as micro analysis tools, were employed to analyze the center at which the damage starts to evolve. The occurrence of rupture at the center also implies that the areas between the grips are subjected to different levels of stress and damage, which resulted in a non-uniform surface along this area. Thus, the contact angle measurements were conducted on the area between the grips to confirm this non-uniformity as illustrated in Fig. 3. Table 3 lists the samples notations and the corresponding testing conditions.

3. Results and discussions

3.1. Mechanical testing

For BW membrane samples under dry, wet (6% water uptake), and wet (33% water uptake) circumstances, Fig. 4 shows the engineering stress against strain curves, and Table 4 summarizes the mechanical properties of the tested membrane samples under different conditions compared to the properties of the polyester (backing layer) alone that was tested in a previous publication [31]. For the purpose of validating repeatability, three identical specimens underwent uniaxial tensile testing under each of the circumstances, and the presented results represent the average values. Specimens under dry conditions exhibited higher rupture strength and higher ductility (elongation to failure). It was noticed that the ultimate tensile strength of BW membrane samples decreased with the increase of the water uptake. This trend of accelerated mechanical degradation indicates the harmful effect of moisture

Table 2
Specifications and operational limits of the tested membrane (BW30LE).

Feed	Brackish Water
Maximum operating pressure (bar)	41
Maximum operating temperature ($^\circ \text{C}$)	45
Maximum feed flow (m^3/h)	19
pH Range (25°C)	2–11
Flux (gfd/psi)	37–46/225
Rejection (2000 ppm NaCl, 10 bar, 25°C)	99.00%

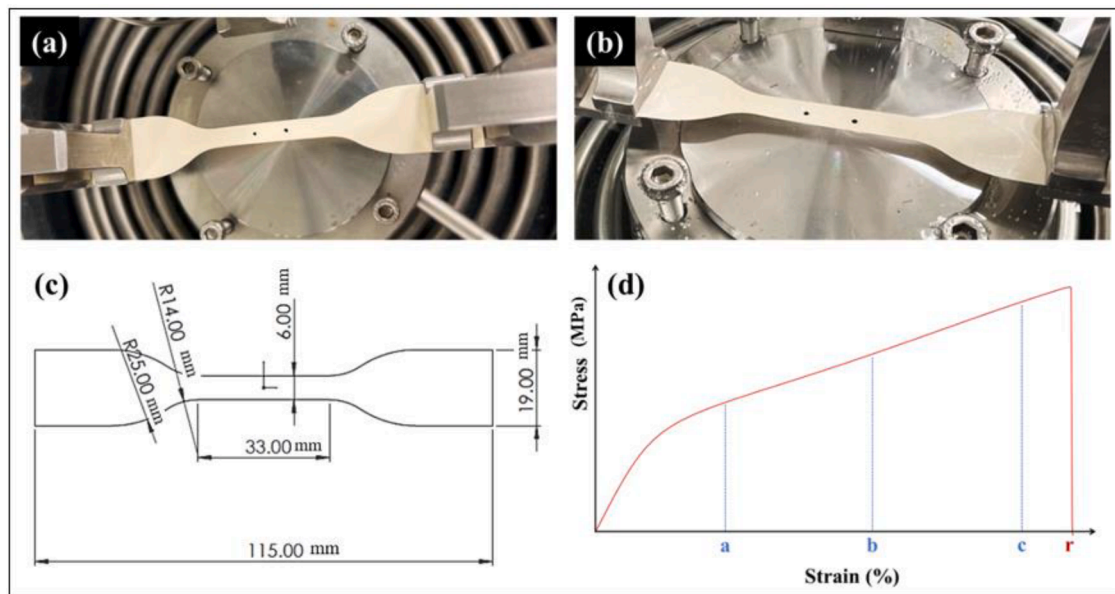


Fig. 2. Uniaxial tensile testing under (a) Dry and (b) Wet conditions, (c) Dimensions for the tensile sample, and (d) illustration of the interrupted tests used in this work where r represents the complete rupture while a, b, and c represent the strain% at which the mechanical test was interrupted.

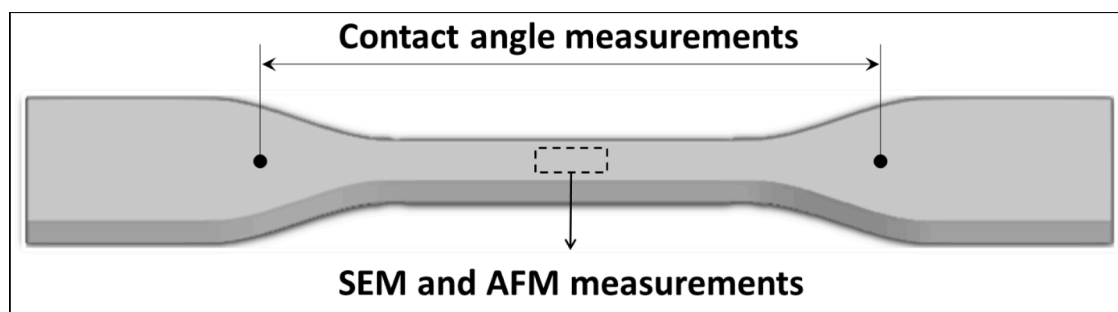


Fig. 3. Illustration of the profiles used for the characterization.

Table 3
Denotation and description of the tested membrane samples.

Notation	Pre-test sample preparation	Testing conditions	Mechanical test
BW	–	–	Unloaded membrane
D ₅	Washing and immersion in DIW followed by overnight drying at RT	Dry @ RT	Interrupted @ 5%
D ₈		Dry @ RT	Interrupted @ 8%
D ₁₁		Dry @ RT	Interrupted @ 11%
D _r		Dry @ RT	Up to rupture
W ₅	Washing and immersion in DIW followed by overnight drying at RT	Wet, immersed in DIW during tensile testing (5 min, 6% water uptake, RT)	Interrupted @ 5%
W ₈			Interrupted @ 8%
W ₁₁			Interrupted @ 11%
W _r			Up to rupture
WI ₅	Washing and immersion in DIW, overnight drying at RT, followed by 24 h immersion in DIW at RT	Wet, immersed in DIW during tensile testing (33% water uptake, RT)	Interrupted @ 5%
WI ₈			Interrupted @ 8%
WI _{9.5}			Interrupted @ 9.5%
WI _r			Up to rupture

absorption on the fracture resistance of the BW membrane. This change in mechanical properties may be attributed to the moisture absorption that weakened the polyester fiber-matrix bondings [35]. The polyester backing layer dominates the membrane's overall behavior and mechanical strength, while the top layers respond differently to the applied stress and are more prone to deformation at significantly lower levels [29,32]. Therefore, it is important to examine the integrity of the selective layer, which is responsible for the performance of the membranes, at different load levels. This is examined in the next sections. The red arrows in Fig. 4 present the strain limits for the controlled interrupted testing under each condition. Then interrupted tensile testing for each condition was conducted up to three defined strain limits: 5, 8, and 11 for dry and wet samples with 6% water uptake and 9.5% for wet samples with 33% water uptake).

3.2. SEM analysis

The SEM analysis is a useful tool for studying the various characteristics of composite membranes, such as their structure, morphology, and properties. One advantage of this tool is that it can provide a direct visual representation of the membrane's morphology and the micro-scale damages. Fig. 5 shows the SEM images of the as-received BW membrane (unloaded) and depicts a rough and leaf-like morphology at high magnifications. This morphology is commonly referred to as the ridge-and-valley and is typically seen in TFC-RO membranes [36]. The SEM images shown in Fig. 6 show the effect of the mechanical stresses

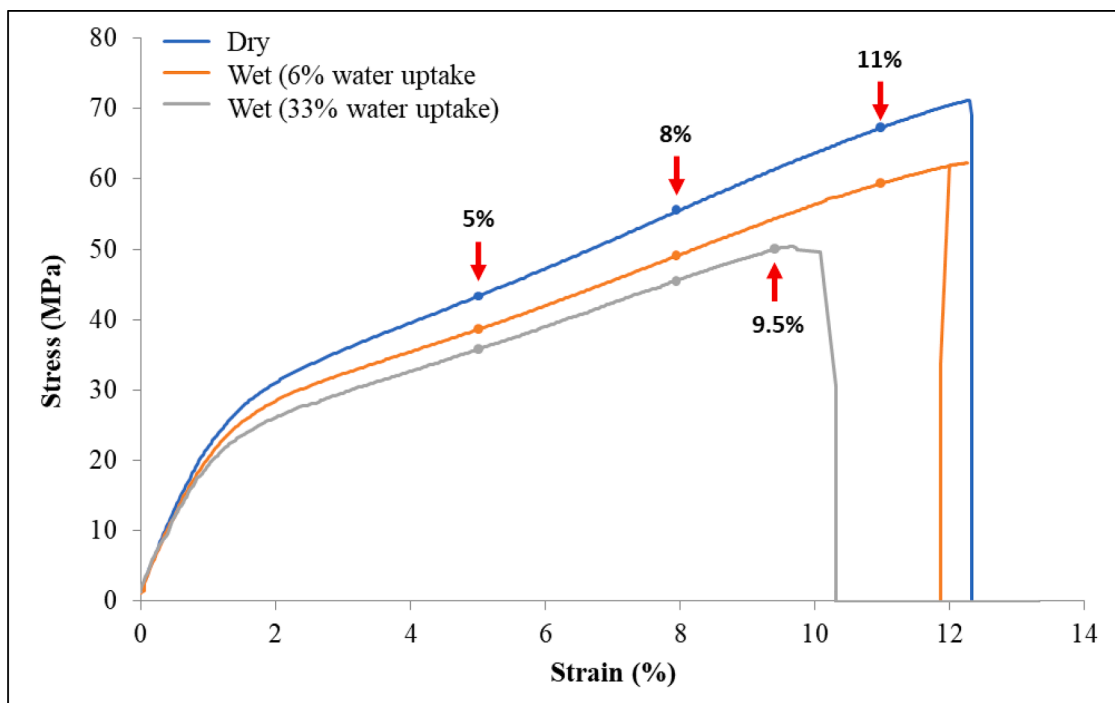


Fig. 4. Engineering stress versus strain curves of BW30 membrane samples under dry and wet (6% and 33% water uptake) conditions.

Table 4

Mechanical properties of BW30 membrane samples under dry and wet conditions (The \pm values represent the standard deviation).

Sample	Modulus of Elasticity (E) (MPa)	Flow Stress (Yield Strength) (MPa)	Ultimate Strength (MPa)	Rupture Stress (MPa)	Rupture Strain (%)
Dry	22.0 \pm 0.4	19.6 \pm 0.5	71.0 \pm 1.2	71.0 \pm 1.2	12.3 \pm 0.5
Wet (6% water uptake)	21.1 \pm 0.6	18.3 \pm 0.7	62.0 \pm 1.6	61.5 \pm 1.6	11.9 \pm 0.7
Wet (33% water uptake)	15.5 \pm 0.4	17.1 \pm 0.4	50.3 \pm 1.5	49.6 \pm 1.6	10.3 \pm 0.5
Polyester	17.4 \pm 0.6	18.7 \pm 0.9	62.5 \pm 2.1	61.6 \pm 2.3	10.7 \pm 0.8

applied on the TFC morphology at four different locations on each sample tested. More locations of damages are presented in Figure S1 in the supplementary information. The images reveal that no serious damages are observed at a 5% strain level under all conditions tested. In the dry conditions, only minor stretches have been observed on D₅ surface as depicted in Fig. 6(a). The magnified images in Fig. 7(a1–a4) show that the TFC layer is still cohesive and is not severely damaged or thinned. When immersed for a short time, the TFC layer exhibited more obvious stretching and thinning as depicted by the W₅ images in Fig. 6(b). The high-magnification images of W₅ in Fig. 7(b1–b4) show that the

thinning became more obvious compared to those observed in dry condition. Upon long time immersion (33% water uptake), the stretches and wrinkles were observed in more locations and became more prevalent in W₁₅ as shown in Figs. 6c and 7(c1–c4). Although no severe cracks or deformations were observed at 5% strain for all conditions tested, the stretching and thinning of the TFC layer can lead to an increase in water and salt permeance through the membrane [29].

At a strain of 8%, the damages became more predominant in all conditions with different severity levels as depicted by Fig. 6. The surface evolution of D₈ and W₈ membranes was almost similar as shown in Fig. 6(a and b). In addition to the increased number of stretches observed, major wrinkles, cracks, and deformations of the TFC layer were observed in some locations. These deformations can be clearly seen in the high-magnification images in Fig. 8(a1–a4) and (b1–b4) for D₈ and W₈, respectively. Upon long immersion, more stretches and wrinkles were observed in different locations as shown in Fig. 6(c). Although these stretches became more prevalent on W₁₈ surface compared to D₈ and W₈, the severity level of these stretches is obviously less. Intense wrinkles were observed in one location on W₁₈ that resulted in an obvious damage in the TFC layer as shown in Fig. 8(c1–c4). Fig. 6(a and b) depicts that at 11% strain which is very close to the rupture strain, more cracks and deformations in the TFC layer were observed on D₁₁ and W₁₁ surfaces. Investigation of these cracks at high magnifications (Fig. 9(a1–a4) and (b1–b4)) showed that the damages were extended to the middle layer by the presence of PSF layer in some locations as shown in Fig. 9(b4). In contrast, less cracks were observed in samples tested under 33% water uptake (W_{19.5}) at which most of the surface evolution

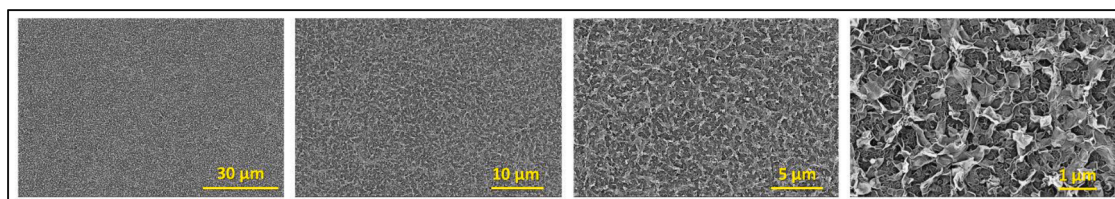


Fig. 5. SEM images of the BW30-LE membrane as received (unloaded, selective layer surface) at magnifications of 4, 8, 16, and 60 kx.

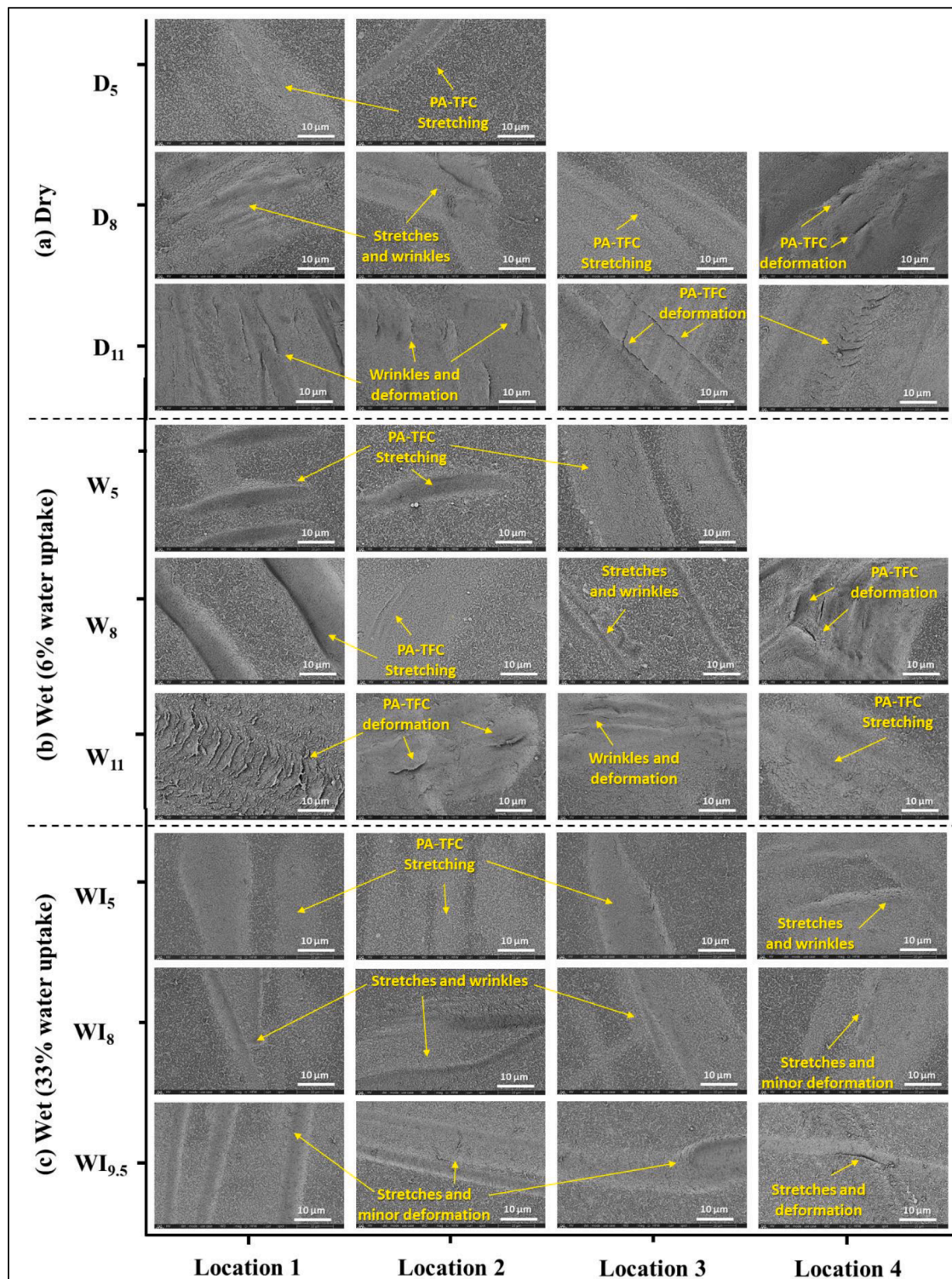


Fig. 6. SEM images showing the types of damages observed in the tested samples (selective layer surface, 8000 X magnification, scale bar is 10 μ m).

was in the form of stretches and wrinkles with varying severity levels as shown in Fig. 6(c) and Fig. 9(c1–c4).

The overall SEM results suggest that the low water uptake does not influence the membrane mechanical integrity and hence they exhibit similar behavior to dry samples. This could be explained by the fact that the 5 min immersion is not enough for membrane wetting and hence doesn't influence the response of the TFC and other layers. After 24 h of immersion, the top composite layer (i.e., PSF-PA) was hydrated and became more stable, and therefore less severe cracks were observed

compared to those tested in dry and after short immersion time. The TFC layer is very thin, rigid, and tightly cross-linked, and hence the hydration has a negligible effect on its geometry and mechanical integrity [37, 38]. On the other hand, the TFC layer geometry and integrity depends mainly on the adhesion properties with the middle layer (i.e., PSF) [13, 19]. Polymer membranes like PSF become ductile when hydrated as water molecules plasticize the polymer matrix [39,40]. Manawi and co-workers [41] found that wet PSF membranes exhibit around 42% higher rupture strain than that of dry PSF. These findings suggest that

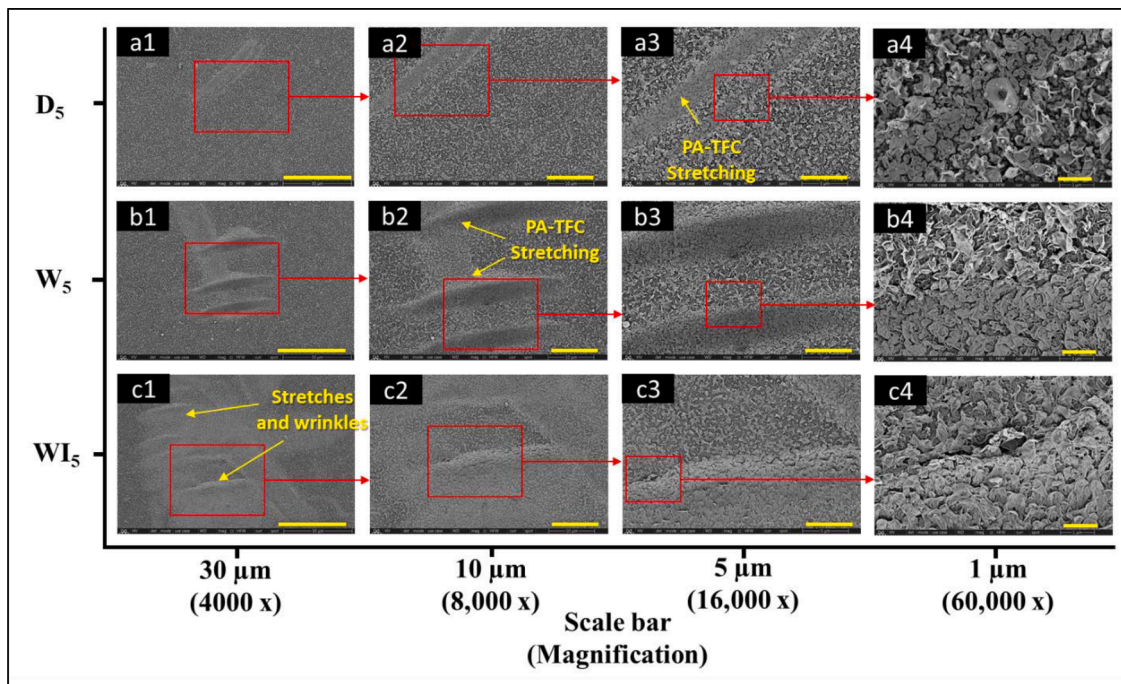


Fig. 7. Surface SEM images of the membrane samples loaded at 5% strain in dry and wet conditions at different magnifications.

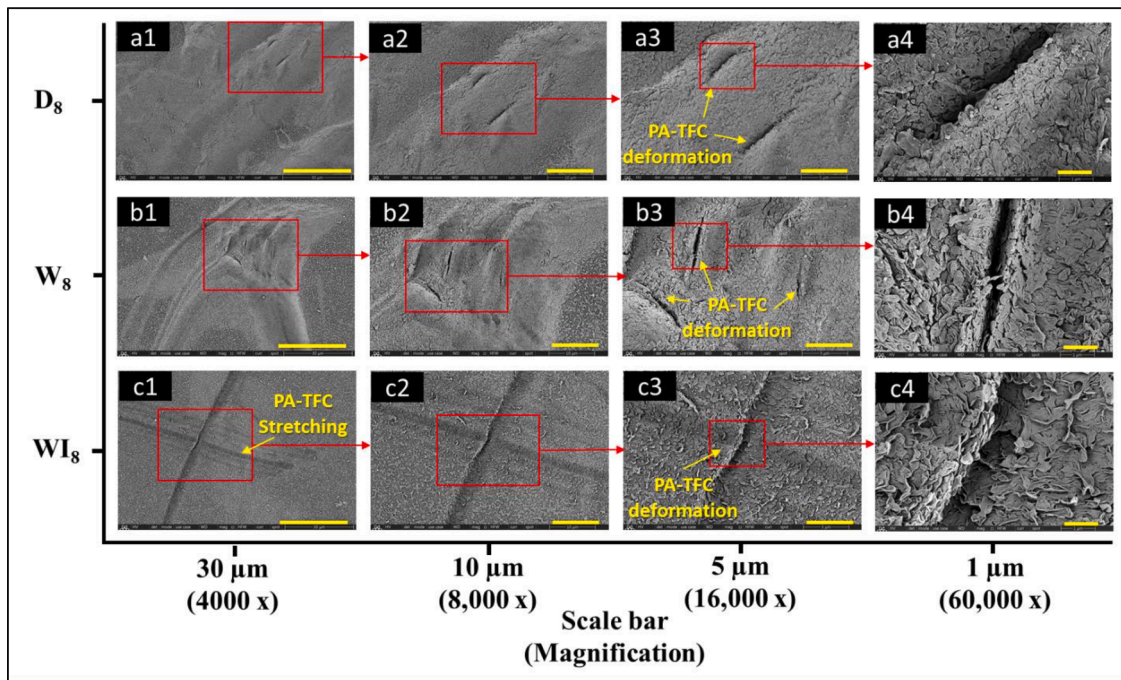


Fig. 8. Surface SEM images of the membrane samples loaded at 8% strain in dry and wet conditions at different magnifications.

the higher stability of TFC layer of membranes with higher water uptake could be attributed to the stability of the wet PSF layer that doesn't experience severe cracks at 8 or 9.5% strains. Hence, the TFC layer remains cohesive owing to the adhesion properties and higher stability of the middle layer. At strain levels higher than 9.5%, the polyester backing starts to fracture (Fig. 4) leading to a complete membrane rupture. The stress-strain curves presented in Fig. 4 showed that the wet membranes fail at lower tensile stress than this of dry membrane. This is attributed to the dominance of the reinforcing polyester backing that have less mechanical strength in wet conditions [42,43]. It has been reported that the

moisture absorption affects the fiber-matrix bondings resulting in lower mechanical strength [35].

Contrastingly, the PSF layer has less ductility in dry conditions, which explains the cracks and deformations observed at strains higher than 8% resulting in more deformations with high severity in the TFC layer. This can be confirmed by the presence of PSF layer at high magnification images in Figs. 8 and 9. Fig. S2 in the supplementary information shows SEM images of scanned areas close to the fracture region for D_r , W_r , and WI_r membranes. These images (Fig. S1 (a1–b4)) show mini cracks and severe wrinkles in the PSF and TFC layers of dry

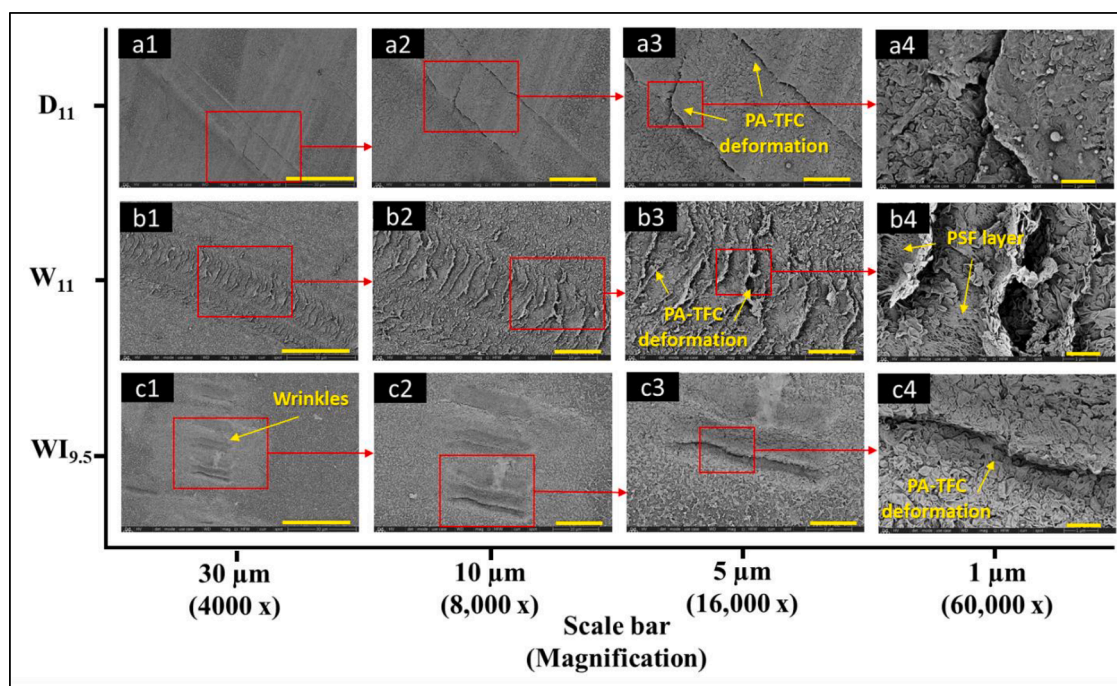


Fig. 9. Surface SEM images of the membrane samples loaded at 11% strain in dry and wet (6% water uptake) and 9.5% strain in wet (33% water uptake) conditions at different magnifications.

and short immersed samples near the rupture region. In the wet sample (Fig. S2 c1–c4), deformation of the TFC layer near the rupture region is also observed with less severity than that of the dry samples. This confirms that the PSF and TFC layers are more cohesive in the wet conditions even at areas near the rupture.

These findings suggest that the PSF and TFC layers exhibit surface damage before the complete membrane fracture in dry conditions, and become more stable when hydrated, and hence the controlled hygro-mechanical testing becomes an essential tool to test its mechanical integrity.

3.3. AFM analysis

AFM is an essential tool and complement to SEM for the morphological characterization of TFC membranes that provides quantified information about the roughness parameters of a membrane surface. Surface roughness can be measured in terms of the average roughness (R_a) and root mean square roughness (RMS or R_q). R_a and RMS roughness are the key physical parameters usually reported to represent the membrane surface roughness. The difference in surface area (SAD) is another essential parameter obtained by AFM analyses which represents the difference between the calculated 3D area (effective area) and the projected area. In general, the higher the RMS and R_a values, the rougher the membrane surface and the larger the effective area of the membrane. It's also worth noting that a larger membrane effective area is always linked to higher water permeability [44]. On the other hand, the rough surface is more prone to foulant accumulation in the valleys, which results in a reduction in the flow rate and the quality of the permeate [45]. Surface roughness is usually altered when a physical or chemical change is applied to the membrane. The chemical changes affecting membrane roughness include fillers addition [46,47], cross-linking [48], substrate modification [13,19], and compositions variation [49].

In this study, the AFM analysis was conducted to explore the morphological changes resulted from the applied stresses. In the absence of chemical modifications, any change in the membrane's roughness can be attributed to the applied stress. Fig. 10 presents the 3D AFM images at

one location of each sample, and the averaged roughness parameters (R_a , R_q , and SAD%) are listed in 5. Fig. S3, S4, and S5 in the supplementary information present the 3D AFM images for membranes tested in dry, wet (6% water uptake), and wet (33% water uptake), respectively, at different locations with the corresponding R_q , R_a , and SAD values. The results showed that the surface of the unloaded membrane (BW) has a uniform peak-valley structure with R_q and SAD values of 54.6 ± 1.6 nm and $39.3 \pm 0.5\%$, respectively. In contrast, the surface became less uniform after applying the stress and the uniformity decreased with the increase of strain stress. The less uniformity of the surface was indicated by the varying roughness and SAD percentages observed at different areas of the same sample. At a 5% and 8% strain, the dry membranes and wet (6% water uptake) (i.e., D_5 , D_8 , W_5 , and W_8) exhibited slight increase in roughness and decrease in SAD values in some areas. The decrease in SAD values is attributed to the stretching of TFC layer. More stretches were observed at 11% strain where the SAD values decreased to 25.3 and 23.3% in some areas of D_{11} and W_{11} , respectively. Membranes with higher water uptake (33%) showed higher levels of non-uniformity at which the SAD values decreased to levels lower than 20% under the interrupted stresses. These findings suggest more intense stretches compared to membranes tested in dry and at 6% water uptake which is in good agreement with the SEM results. These stretches can be clearly visualized by the 3D AFM images in Fig. 10(j–m). The increase in R_q is usually associated with an increase in SAD value [44]. However, it has been observed in some areas that SAD value decreases slightly or remains unchanged while R_q is higher than this of the unloaded membrane as shown in Fig. 10(c,g,e and i). This could be explained by the sharp and localized peaks stretching within the scanned area resulting in higher deviation from the mean plane (i.e., R_q). These localized stretches result in severe wrinkles and cracks which agrees with the SEM observations and can be visualized in the 3D images obtained at these locations (Fig. 10(c,g,e and i)). On the other hand, the stretching covers the whole scanned area of the samples immersed overnight which decreases both the roughness and SAD values. These observations are in good agreement with the SEM observations, which showed that the surface damage of the TFC of dry and less hydrated membranes are in the form of localized cracks and severe wrinkles,

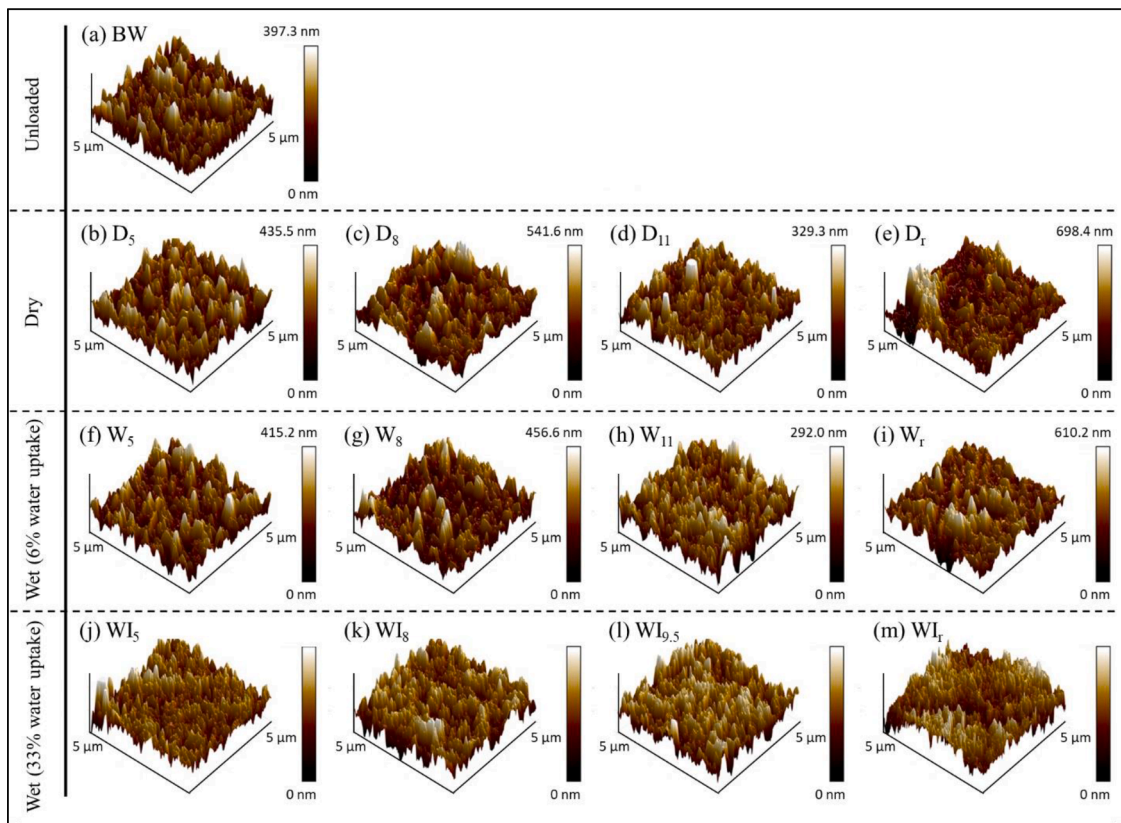


Fig. 10. 3D AFM images of the membrane samples tested under different conditions.

whereas the surface damage observed at 33% water uptake were in the form of widespread stretches and less-severity wrinkles.

3.4. Contact angle analysis

Contact angle is a useful tool to measure of wettability and hydrophilicity of a membrane surface [50]. Membrane hydrophilicity plays a vital role in determining the efficiency of its separation and fouling properties. It is generally believed that the higher the degree of surface hydrophilicity, the higher the membrane's permeability [44]. Like the roughness properties, the surface's morphology and chemistry can also affect its hydrophilicity [51]. Therefore, a change in the membrane hydrophilicity can also indicate a change in its surface geometry when no chemical change is present. In this work, the contact angle was

measured to indicate the morphological change in membrane surface caused by the mechanical stress applied. The average contact angle of the tested samples are illustrated in Fig. 11 and listed in Table 5. The error bars in Fig. 11 correspond to the standard deviation (SD) of contact angles tested at these locations. As the measured area is subjected to different levels of stress, the SD value was used to indicate the non-uniformity of CA profile within each sample. The unloaded membrane (BW) showed an average contact angle of $54.9 \pm 0.9^\circ$. The low SD value of the unloaded membrane indicates high uniformity of contact angles through its surface. Contrastingly, the stressed membranes showed higher levels of uncertainty as demonstrated by their SD values. These uncertainties suggest that the uniformity of these surfaces was altered due to the stress applied.

Fig. 12 illustrates the localized contact angle measured at every point

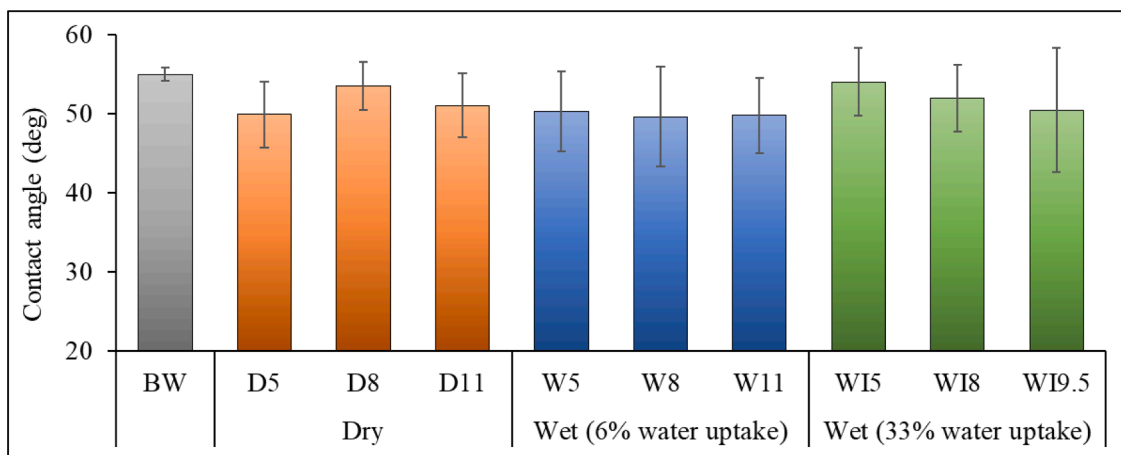


Fig. 11. The average contact angle of the tested membrane samples. The error bars correspond to standard deviation of the locations tested ($n = 10$).

Table 5

Average roughness parameters and contact angle (CA) of the tested membranes. The \pm values represent the standard deviation ($n = 3$ for roughness parameters and $n = 10$ for CA measurements).

Membrane	Rq (nm)	Ra (nm)	SAD (%)	CA (deg)
BW	54.6 \pm 1.6	43.5 \pm 1.3	39.3 \pm 0.5	54.9 \pm 0.9
D ₅	66.7 \pm 2.9	53.2 \pm 2.2	34.6 \pm 0.3	49.9 \pm 4.4
D ₈	74.5 \pm 5.4	58.2 \pm 4.3	36.0 \pm 2.6	53.5 \pm 3.2
D ₁₁	60.5 \pm 10.4	47.6 \pm 8.5	34.4 \pm 6.9	51.0 \pm 4.2
D _r *	68.1 \pm 21.6	52.5 \pm 17.0	36.0 \pm 9.9	–
W ₅	62.7 \pm 2.4	49.6 \pm 2.1	35.3 \pm 1.3	50.3 \pm 5.4
W ₈	62.2 \pm 1.8	49.2 \pm 1.1	33.8 \pm 0.6	49.6 \pm 6.6
W ₁₁	60.5 \pm 18.6	47.4 \pm 12.9	27.6 \pm 3.6	49.8 \pm 5.0
W _r *	68.0 \pm 6.5	52.0 \pm 4.1	35.1 \pm 1.7	–
W ₁₅	45.6 \pm 11.4	36.0 \pm 9.1	22.2 \pm 5.4	54.0 \pm 4.6
W ₁₈	48.8 \pm 10.4	39.2 \pm 8.1	25.6 \pm 6.1	52.0 \pm 4.4
W _{19.5}	43.3 \pm 10.0	34.8 \pm 7.3	21.7 \pm 4.1	50.4 \pm 8.3
W _{1r} *	39.7 \pm 17.2	31.4 \pm 13.6	18.9 \pm 9.7	–

* Roughness parameters of the ruptured samples (D_r, W_r, and W_{1r}) were estimated at areas near the rupture.

on the tested samples. Clearly, the stressed membranes have non-uniform contact angle profile across the area tested. The results also suggest that W_{19.5} have the highest degree of non-uniformity compared to the other membranes that could be attributed to the prevalence of stretches across the stressed membrane. This non-uniformity of surface can be also indicated by the presence of asymmetric drops in several locations on the stressed samples at which the left and right contact angles of the same drop are unequal (Fig. 13). It is widely accepted that the surface roughness affects its contact angle and its symmetry [47,52]. Therefore, the non-uniformity and asymmetry of the measured contact angle on the stressed samples can be attributed to the change in their roughness properties as revealed by the AFM results.

4. Conclusions

TFC membranes have proven their high efficiency in many

membrane-based processes. However, the TFC layer is very sensitive and tends to undergo severe deformations owing to the complex stresses applied at varying conditions. Efforts in exploring the mechanical stability and integrity of TFC membranes are limited. Aiming to have a better understanding of their mechanical integrity, the evolution and response of TFC layer to controlled interrupted uniaxial tensile testing was investigated. The mechanical stresses were applied under dry and wet conditions with 6% and 33% water uptake. It has been demonstrated that the structural integrity and surface functionality of the TFC layer were severely affected when subjected to strain limits lower than the strain-rupture stresses. The key findings of this work are described below:

- (1) Dry membranes have higher strain levels at rupture ($\sim 12\%$) than that of wet membranes ($\sim 10\%$). This behavior was attributed to the weaker fiber matrix bonding of the polyester layer in wet conditions.
- (2) The failure of the TFC layer occurs at much lower strain levels than the rupture-strain.
- (3) Samples tested under dry and short immersion time exhibit the same behavior under mechanical stress. This suggests that low water uptake (6%) does not influence the mechanical properties of the membrane.
- (4) At a strain limit of 5% and under dry and wet conditions, the effect on the TFC layer was in the form of minor stretches and thinning with no obvious cracks or deformations.
- (5) At strain levels higher than half the rupture strain, severe wrinkles and localized deformations in the TFC layer were observed with membranes tested under dry and low water uptake level (6%). The SEM results showed that the damage was also extended to the middle layer as evidenced by the change in appearance of the porous PSF matrix in some locations at high magnifications.
- (6) Wet membranes immersed overnight (33% water uptake) showed lower severity damages even at strain limits as high as 9.5% than those observed in dry and wet (6% water uptake). The damages

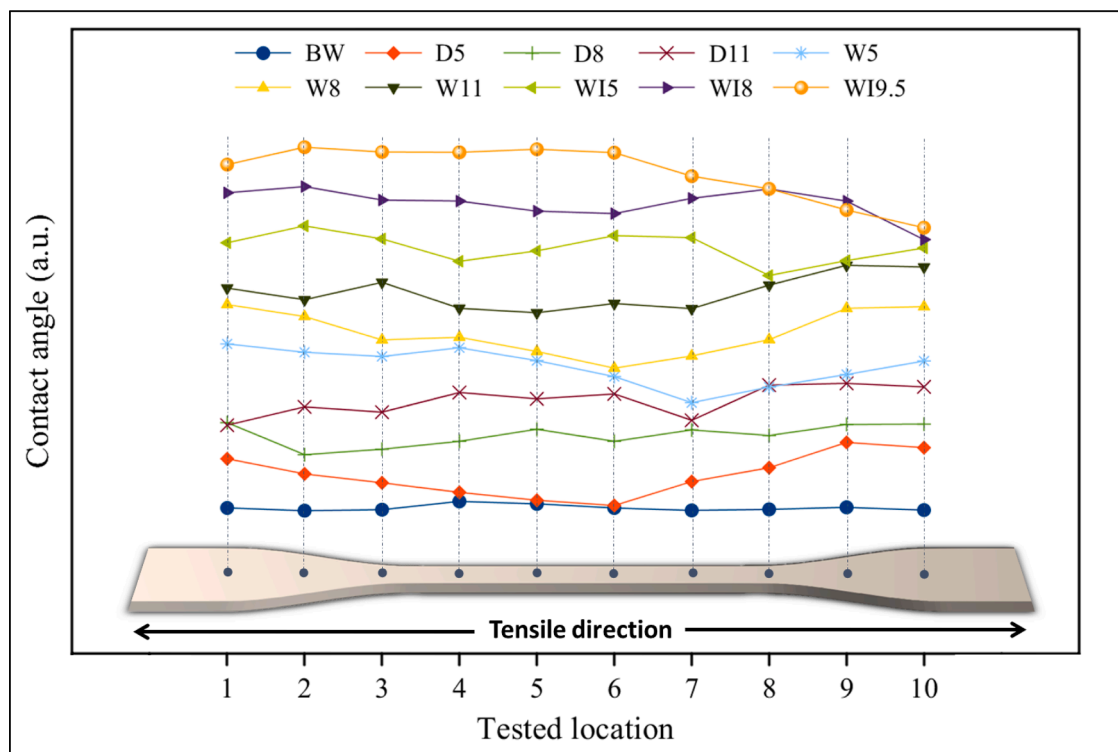


Fig. 12. Illustration of the contact angle profile on the tested points of each sample. Measurements were stacked vertically for clarity.

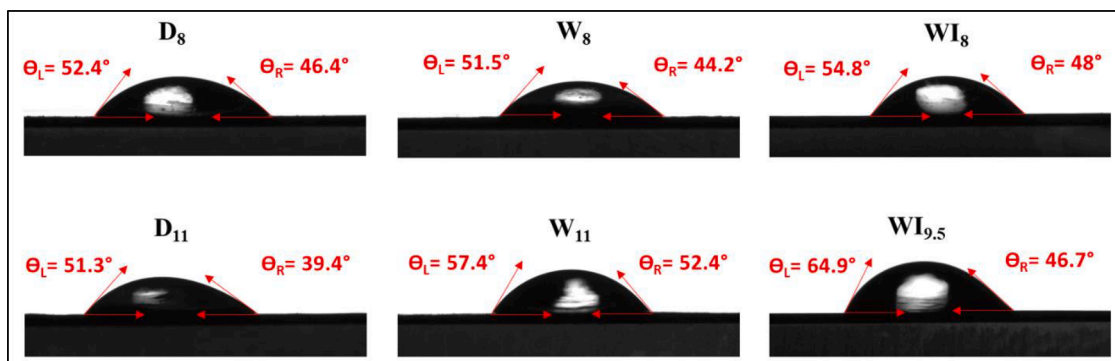


Fig. 13. Contact angle images showing asymmetric drops observed at various locations on the mechanically stressed samples in wet and dry conditions.

were in the form of widespread stretches and wrinkles with fewer cracks or deformations.

- (7) The results were supported by the contact angle and AFM findings which showed that the membrane surface becomes less uniform when subjected to different strain limits under different conditions. The AFM results suggested also that the damages in dry and wet (6% water uptake) conditions are localized and severe, while they are more prevalent with less severity with samples tested under higher water uptake levels (33%).
- (8) The combination of strain-rupture results with the SEM and AFM findings suggest that each layer behave differently under the tested conditions. Polyester backing has less mechanical strength in wet conditions due to the weaker bonding of fibers, while water molecules plasticize the PSF matrix providing higher ductility and stability to the top composite layer (PSF-PA).

The findings of this study suggest that the complexity of the loading conditions under which membranes are commonly used calls for further investigations to better simulate real operating conditions in the lab environment. The results of this work provide a better understanding and prediction of how the surface characteristics of the TFC layer behave and evolve under different mechanical load levels and conditions. The methods proposed here apply to different TFC membranes used in various water treatment and desalination applications. As this study is the first to investigate the evolution of surface damage of TFC layers under different strain limits under different conditions, it also highlights the need to do more investigations under real operating conditions such as acidic/basic conditions, non-uniaxial loading, and different temperature levels.

Declaration of Competing Interest

The authors declare that they have no known competing financial interests or personal relationships that could have appeared to influence the work reported in this paper.

Data availability

Data will be made available on request.

Acknowledgement

Open access funding is provided by Qatar National Library.

Supplementary materials

Supplementary material associated with this article can be found, in the online version, at [doi:10.1016/j.surf.2023.102911](https://doi.org/10.1016/j.surf.2023.102911).

References

- [1] H. Isawi, Development of thin-film composite membranes via radical grafting with methacrylic acid/ZnO doped TiO₂ nanocomposites, *React. Funct. Polym.* 131 (2018) 400–413, <https://doi.org/10.1016/J.REACTFUNCTPOLYM.2018.08.018>.
- [2] A.K. Rana, V.K. Gupta, A.K. Saini, S.I. Voicu, M.H. Abdellattifaand, V.K. Thakur, Water desalination using nanocelluloses/cellulose derivatives based membranes for sustainable future, *Desalination* 520 (2021), 115359, <https://doi.org/10.1016/J.DESAL.2021.115359>.
- [3] H. Albatrni, H. Qiblawey, M.H. El-Naas, Comparative study between adsorption and membrane technologies for the removal of mercury, *Sep. Purif. Technol.* 257 (2021), 117833, <https://doi.org/10.1016/j.seppur.2020.117833>.
- [4] M. al-Shaeli, R.A. Al-Juboori, S. al Aani, B.P. Ladewig, N. Hilal, Natural and recycled materials for sustainable membrane modification: recent trends and prospects, *Sci. Total Environ.* 838 (2022), 156014, <https://doi.org/10.1016/J.SCITOTENV.2022.156014>.
- [5] M.S. Abdul Wahab, A.A. Ghazali, N.F. Abd Ghapar, S. Abd Rahman, R. Abu Samah, Thin film nanocomposite (Tfnc) membranes: future direction of Tfnc synthesis for alcohol dehydration, *Surf. Interfaces* 25 (2021), 101165, <https://doi.org/10.1016/J.SURFIN.2021.101165>.
- [6] A. Mazumder, Z. Chowdhury, D. Sen, C. Bhattacharjee, Estimation of membrane fouling and its alleviation with novel biocidal silver coordinated metallosurfactant cleaning solution, *Surf. Interfaces* 26 (2021), 101360, <https://doi.org/10.1016/J.SURFIN.2021.101360>.
- [7] A. Alkhouzaam, H. Qiblawey, Functional GO-based membranes for water treatment and desalination: fabrication methods, performance and advantages. A review, *Chemosphere* (2021) 274, <https://doi.org/10.1016/j.chemosphere.2021.129853>.
- [8] N.H. Zainal Abidin, S.N.A. Shafie, H. Suhaimi, N.S. Sambudi, N.A.H. Sapiaa Md Nordin, Incorporation of carboxyl and amino functionalized carbon quantum dots in thin film membrane for nanofiltration, *Polym. Test.* 100 (2021), 107270, <https://doi.org/10.1016/J.POLYMTESTING.2021.107270>.
- [9] M.R. Moradi, M. Pourafshari Chenar, S.H. Noie, M. Hesampour, M. Mänttäri, PDMS coating of used TFC-RO membranes for O₂/N₂ and CO₂/N₂ gas separation applications, *Polym. Test.* 63 (2017) 101–109, <https://doi.org/10.1016/J.POLYMTESTING.2017.07.024>.
- [10] L. Miao, T. Jiang, S. Lin, T. Jin, J. Hu, M. Zhang, Y. Tu, G. Liu, Asymmetric forward osmosis membranes from p-aramid nanofibers, *Mater. Des.* 191 (2020), 108591, <https://doi.org/10.1016/J.MATDES.2020.108591>.
- [11] X. Li, S. Zhang, F. Fu, T.S. Chung, Deformation and reinforcement of thin-film composite (TFC) polyamide-imide (PAI) membranes for osmotic power generation, *J. Membr. Sci.* 434 (2013) 204–217, <https://doi.org/10.1016/J.MEMSCI.2013.01.049>.
- [12] A. Ullah, H.J. Tanudjaja, M. Ouda, S.W. Hasan, J.W. Chew, Membrane fouling mitigation techniques for oily wastewater: a short review, *J. Water Process Eng.* 43 (2021), 102293, <https://doi.org/10.1016/J.JWPE.2021.102293>.
- [13] E. Tian, X. Wang, Y. Zhao, Y. Ren, Middle support layer formation and structure in relation to performance of three-tier thin film composite forward osmosis membrane, *Desalination* 421 (2017) 190–201, <https://doi.org/10.1016/J.DESAL.2017.02.014>.
- [14] F. Liu, L. Wang, D. Li, Q. Liu, B. Deng, Preparation and characterization of novel thin film composite nanofiltration membrane with PVDF tree-like nanofiber membrane as composite scaffold, *Mater. Des.* 196 (2020), 109101, <https://doi.org/10.1016/J.MATDES.2020.109101>.
- [15] S. Zhang, F. Fu, T.S. Chung, Substrate modifications and alcohol treatment on thin film composite membranes for osmotic power, *Chem. Eng. Sci.* 87 (2013) 40–50, <https://doi.org/10.1016/J.CES.2012.09.014>.
- [16] K. Wang, A.A. Abdalla, M.A. Khaleel, N. Hilal, M.K. Khraisheh, Mechanical properties of water desalination and wastewater treatment membranes, *Desalination* 401 (2017) 190–205, <https://doi.org/10.1016/J.DESAL.2016.06.032>.
- [17] Q.M. Li, H.Y. Ma, Y.N. Hu, Y.F. Guo, L.J. Zhu, Z.X. Zeng, G. Wang, Polyamide thin-film composite membrane on polyethylene porous membrane: fabrication, characterization and application in water treatment, *Mater. Lett.* 287 (2021), 129270, <https://doi.org/10.1016/J.MATLET.2020.129270>.

- [18] S.H. Park, S.J. Kwon, M.G. Shin, M.S. Park, J.S. Lee, C.H. Park, H. Park, J.H. Lee, Polyethylene-supported high performance reverse osmosis membranes with enhanced mechanical and chemical durability, *Desalination* 436 (2018) 28–38, <https://doi.org/10.1016/J.DESAL.2018.02.007>.
- [19] Y. Li, R. Wang, S. Qi, C. Tang, Structural stability and mass transfer properties of pressure retarded osmosis (PRO) membrane under high operating pressures, *J. Membr. Sci.* 488 (2015) 143–153, <https://doi.org/10.1016/J.MEMSCI.2015.04.030>.
- [20] M. Namvar-Mahboub, M. Pakizeh, Development of a novel thin film composite membrane by interfacial polymerization on polyetherimide/modified SiO₂ support for organic solvent nanofiltration, *Sep. Purif. Technol.* 119 (2013) 35–45, <https://doi.org/10.1016/J.SEPPUR.2013.09.003>.
- [21] H. Mahdavi, M. Moslehi, A new thin film composite nanofiltration membrane based on PET nanofiber support and polyamide top layer: preparation and characterization, *J. Polym. Res.* 23 (2016) 257, <https://doi.org/10.1007/s10965-016-1157-4>.
- [22] S.J. Kwon, S.H. Park, M.G. Shin, M.S. Park, K. Park, S. Hong, H. Park, Y.I. Park, J. H. Lee, Fabrication of high performance and durable forward osmosis membranes using mussel-inspired polydopamine-modified polyethylene supports, *J. Membr. Sci.* 584 (2019) 89–99, <https://doi.org/10.1016/J.MEMSCI.2019.04.074>.
- [23] J. Wei, Y. Li, L. Setiawan, R. Wang, Influence of macromolecular additive on reinforced flat-sheet thin film composite pressure-retarded osmosis membranes, *J. Membr. Sci.* 511 (2016) 54–64, <https://doi.org/10.1016/J.MEMSCI.2016.03.046>.
- [24] J. Ren, B. O'Grady, G. deJesus, J.R. McCutcheon, Sulfonated polysulfone supported high performance thin film composite membranes for forward osmosis, *Polymer* 103 (2016) 486–497, <https://doi.org/10.1016/J.POLYMER.2016.02.058>.
- [25] M. Obaid, Z.K. Ghouri, O.A. Fadali, K.A. Khalil, A.A. Almajid, N.A. Barakat, Amorphous SiO₂ NP-incorporated oly(vinylidene fluoride) electrospun nanofiber membrane for high flux forward osmosis desalination, *ACS Appl. Mater. Interfaces* 8 (2016) 4561–4574, <https://doi.org/10.1021/acsami.5b09945>.
- [26] A.R. Greenberg, V.P. Khare, W.B. Krantz, Development of a Technique for the in-situ Measurement of the Mechanical Properties of Ultra-Thin Interfacially Polymerized Films, *MRS Online Proc. Libr.* 356 (1994) 541–546, <https://doi.org/10.1557/PROC-356-541>.
- [27] I.J. Roh, J.J. Kim, S.Y. Park, Mechanical properties and reverse osmosis performance of interfacially polymerized polyamide thin films, *J. Membr. Sci.* 197 (2002) 199–210, [https://doi.org/10.1016/S0376-7388\(01\)00623-8](https://doi.org/10.1016/S0376-7388(01)00623-8).
- [28] S. Wang, K. Gu, J. Wang, Y. Zhou, C. Gao, Enhanced the swelling resistance of polyamide membranes with reinforced concrete structure, *J. Membr. Sci.* 575 (2019) 191–199, <https://doi.org/10.1016/J.MEMSCI.2019.01.020>.
- [29] J.A. Idarraga-Mora, A.D. O'Neal, M.E. Pfeiler, D.A. Ladner, S.M. Husson, Effect of mechanical strain on the transport properties of thin-film composite membranes used in osmotic processes, *J. Membr. Sci.* 615 (2020), 118488, <https://doi.org/10.1016/J.MEMSCI.2020.118488>.
- [30] N.N. Bui, J.R. McCutcheon, Nanofiber supported thin-film composite membrane for pressure-retarded osmosis, *Environ. Sci. Technol.* 48 (2014) 4129–4136, <https://doi.org/10.1021/es4037012>.
- [31] F.G. Alabtah, A. Alkhouzaam, M. Khraisheh, New insights into the mechanical behavior of thin-film composite polymeric membranes, *Polymers* 14 (2022), <https://doi.org/10.3390/polym14214657>.
- [32] F.G. Alabtah, A. Alkhouzaam, M. Khraisheh, H. Attia, Characterization of surface properties of thin film composite (TFC) membranes under various loading conditions, *CIRP Ann.* (2022), <https://doi.org/10.1016/J.CIRP.2022.04.069>.
- [33] B. Li, X.X. Ke, Z.H. Yuan, L. Bin Zhong, Q.B. Zhao, Y.M. Zheng, High performance electrospun thin-film composite forward osmosis membrane by tailoring polyamide active layer with polydopamine interlayer for desulfurization wastewater desalination, *Desalination* 534 (2022), 115781, <https://doi.org/10.1016/J.DESAL.2022.115781>.
- [34] E.S. Kim, Y.J. Kim, Q. Yu, B. Deng, Preparation and characterization of polyamide thin-film composite (TFC) membranes on plasma-modified polyvinylidene fluoride (PVDF), *J. Membr. Sci.* 344 (2009) 71–81, <https://doi.org/10.1016/J.MEMSCI.2009.07.036>.
- [35] T. Ramakrishnan, S. Senthil Kumar, S.J. Samuel Chelladurai, S. Gnanasekaran, N. K. Geetha, R. Arthanari, B. Debtera, Effect of moisture content on mechanical properties of AAM natural fiber-reinforced isophthalic polyester composites, *Adv. Mater. Sci. Eng.* 2022 (2022), 3533143, <https://doi.org/10.1155/2022/3533143>.
- [36] L.E. Peng, Z. Yang, L. Long, S. Zhou, H. Guo, C.Y. Tang, A critical review on porous substrates of TFC polyamide membranes: mechanisms, membrane performances, and future perspectives, *J. Membr. Sci.* 641 (2022), 119871, <https://doi.org/10.1016/J.MEMSCI.2021.119871>.
- [37] F. Foglia, B. Frick, M. Nania, A.G. Livingston, J.T. Cabral, Multimodal confined water dynamics in reverse osmosis polyamide membranes, *Nat. Commun.* 13 (2022), 2809, <https://doi.org/10.1038/s41467-022-30555-6>.
- [38] V. Freger, Swelling and morphology of the skin layer of polyamide composite membranes: an atomic force microscopy study, *Environ. Sci. Technol.* 38 (2004) 3168–3175, <https://doi.org/10.1021/es034815u>.
- [39] Z. Cui, X. Tang, W. Li, H. Liu, J. Zhang, H. Wang, J. Li, EVOH in situ fibrillation and its effect of strengthening, toughening and hydrophilic modification on PVDF hollow fiber microfiltration membrane via TIPS process, *J. Mater. Sci.* 54 (2019) 5971–5987, <https://doi.org/10.1007/s10853-018-03281-y>.
- [40] T.D. Tap, D.D. Khiem, L.L. Nguyen, N.Q. Hien, L.Q. Luan, P.B. Thang, S. Ichi Sawada, S. Hasegawa, Y. Maekawa, Humidity and temperature effects on mechanical properties and conductivity of graft-type polymer electrolyte membrane, *Radiat. Phys. Chem.* 151 (2018) 186–191, <https://doi.org/10.1016/J.RADPHYSCH.2018.06.033>.
- [41] Y.M. Manawi, K. Wang, V. Kochkodan, D.J. Johnson, M.A. Atieh, M.K. Khraisheh, Engineering the surface and mechanical properties of water desalination membranes using ultralong carbon nanotubes, *Membranes* 8 (2018), 106, <https://doi.org/10.3390/membranes8040106>.
- [42] M. Hamdan, J. Siregar, T. Cionita, J. Jaafar, A. Efriyohadi, R. Junid, A. Kholil, Water absorption behaviour on the mechanical properties of woven hybrid reinforced polyester composites, *Int. J. Adv. Manuf. Technol.* 104 (2019) 1075–1086, <https://doi.org/10.1007/s00170-019-03976-9>.
- [43] H. Abrial, D. Kadriadi, A. Rodianus, P. Mastariyanto, Ilhamdi, S. Arief, S.M. Sapuan, M.R. Ishak, Mechanical properties of water hyacinth fibers–polyester composites before and after immersion in water, *Mater. Des.* 58 (2014) 125–129, doi:10.1016/J.MATDES.2014.01.043.
- [44] W.J. Lau, A.F. Ismail, P.S. Goh, N. Hilal, B.S. Ooi, Characterization methods of thin film composite nanofiltration membranes, *Sep. Purif. Rev.* 44 (2015) 135–156, <https://doi.org/10.1080/15422119.2014.882355>.
- [45] Z. Xu, J. Zhang, M. Shan, Y. Li, B. Li, J. Niu, B. Zhou, X. Qian, Organosilane-functionalized graphene oxide for enhanced antifouling and mechanical properties of polyvinylidene fluoride ultrafiltration membranes, *J. Membr. Sci.* 458 (2014) 1–13, <https://doi.org/10.1016/j.memsci.2014.01.050>.
- [46] J. Yin, E.S. Kim, J. Yang, B. Deng, Fabrication of a novel thin-film nanocomposite (TFN) membrane containing MCM-41 silica nanoparticles (NPs) for water purification, *J. Membr. Sci.* 423–424 (2012) 238–246, <https://doi.org/10.1016/J.MEMSCI.2012.08.020>.
- [47] A. Alkhouzaam, H. Qiblawey, Novel polysulfone ultrafiltration membranes incorporating polydopamine functionalized graphene oxide with enhanced flux and fouling resistance, *J. Membr. Sci.* 620 (2021), 118900, <https://doi.org/10.1016/j.memsci.2020.118900>.
- [48] X.Y. Chi, B.G. Xia, Z.L. Xu, M.X. Zhang, Impact of cross-linked chitosan sublayer structure on the performance of TFC FO PAN nanofiber membranes, *ACS Omega* 3 (2018) 13009–13019, <https://doi.org/10.1021/acsomega.8b01201>.
- [49] T. Wang, H. Qiblawey, S. Judd, A. Benamor, M.S. Nasser, A. Mohammadian, Fabrication of high flux nanofiltration membrane via hydrogen bonding based co-deposition of polydopamine with poly(vinyl alcohol), *J. Membr. Sci.* 552 (2018) 222–233, <https://doi.org/10.1016/j.memsci.2018.02.009>.
- [50] K.L. Andrade, F.L. Fanta, R.M. do Nascimento, R.S. Cunha, D. Bresolin, E. Diz Acosta, R.A.F. Machado, Wettability tuning of natural rubber/polyvinylpyrrolidone electrospun nonwoven mats, *Surf. Interfaces* 32 (2022), 102129, <https://doi.org/10.1016/J.SURFIN.2022.102129>.
- [51] C. Liu, Y. Guo, Y. Zhou, B. Yang, K. Xiao, H.Z. Zhao, High-hydrophilic and antifouling reverse osmosis membrane prepared based an unconventional radiation method for pharmaceutical plant effluent treatment, *Sep. Purif. Technol.* 280 (2022), 119838, <https://doi.org/10.1016/J.SEPPUR.2021.119838>.
- [52] E. Fontanarova, V. Grosso, S.A. Aljlil, M.A. Bahattab, D. Vuono, F.P. Nicoletta, E. Curcio, E. Di Profio, Effect of functional groups on the properties of multiwalled carbon nanotubes/polyvinylidene fluoride composite membranes, *J. Membr. Sci.* 541 (2017) 198–204, <https://doi.org/10.1016/j.memsci.2017.07.002>.